



Subject Areas:

mathematical modelling, mechanics,
wave motion

Keywords:

dispersion relation, dominant
balance, elastic wave, group velocity,
negative Poisson's ratio, ring
frequency

Author for correspondence:

C. J. Chapman

e-mail: c.j.chapman@keele.ac.uk

A Poisson scaling approach to backward wave propagation in a tube

C. J. Chapman¹ and S. V. Sorokin²

¹Department of Mathematics, University of Keele,
Staffordshire ST5 5BG, UK

²Faculty of Engineering and Science, Aalborg
University, Fibigerstraede 16, 9220 Aalborg, Denmark

A mathematical analysis of wave propagation along an elastic cylindrical tube is presented, with the aim of determining the range of Poisson's ratio for which backward wave propagation (i.e. at negative group velocity) can occur near the ring frequency. This range includes zero Poisson's ratio and a surrounding interval of positive and negative values, whose width depends on the thickness of the tube. The whole range of Poisson's ratio is considered, so that the work applies to modern materials, e.g. composites. All results are presented in simple analytic form by means of a dominant balance in parameter space. The identification of this balance, which is unique, is a main new result in the paper, which makes possible a new type of shell theory based on 'Poisson scaling'. The mathematical approach is deductive from the equations of motion, rather than being based on kinematic hypotheses. A key finding, accessible via the Poisson scaling, is that the regime of negative group velocities extends to high wavenumbers, while being confined to a narrow band of frequencies. Thus responses localised in space are possible for near-monochromatic forcing, an important fact for nonlinear theories of tube dynamics near the ring frequency.

1. Introduction

The starting point of this paper is a mathematical method developed in [1] for analysing the dispersion relation for elastic waves propagating along a tube. The idea of the method is that by exploiting a set of recurrence relations among the higher Wronskians of the underlying differential equations, and expanding in powers of the dimensionless thickness of the tube, a compact set of polynomial equations is obtained, from which many

analytic deductions about the nature of the wave propagation along the tube are possible.

In particular, it was shown that near the ring frequency for axisymmetric waves there is a regime of negative group velocity, i.e. backward wave propagation, and results were presented for the limiting cases of very small wavenumber or Poisson's ratio. However, backward propagation is not restricted to these limits, and given the importance of the neighbourhood of the ring frequency [2], it seems worthwhile to give a full account of the dispersion curve nearby, over the maximum parameter range permitted by the theory. Such an account is presented here. We provide analytical results in the two-dimensional parameter space (ν, ϵ) , where ν is Poisson's ratio of the elastic material forming the tube wall, and ϵ is its dimensionless thickness. The results include a precise analytical description of the arc of negative group velocity in the (frequency, wavenumber) plane, including the position of its endpoints and an accurate calculation of a quantity we call the frequency overhang. This is the length of the projection onto the frequency axis of the arc of the dispersion curve on which the group velocity is negative. A glance at figure 2 will reveal why this terminology is appropriate. Our formulae are simpler than those currently available for related examples of backward propagation [3–5].

In the course of the work, we performed numerical experiments to determine the range of accuracy of the mathematical technique of dominant balance [6–8] which we have used. Here, the technique requires us to determine the exponent α which maximises the number of terms in balance when $\nu \sim \epsilon^\alpha$. The answer unambiguously is that $\alpha = 1$, which means that results may be expressed in terms of a scaled Poisson's ratio of order ν/ϵ . Approximations based on this 'Poisson scaling' are found to be accurate over a wide range of ν and ϵ covering all values likely to arise in practice, including large values. Accordingly, we give the scaling some prominence.

The Poisson scaling approach is new in the theory of elastic waves, and we believe it offers scope for new forms of shell theory in which it is adopted at the outset in the energy functional chosen, thus extending to thicker shells the theory in such classical works as [9]. Although we concentrate on the frequencies and wavenumbers for which backward propagation occurs, the method of Poisson scaling is in fact general; it may be used at any frequency and wavenumber, and also in nonlinear elastic problems [10,11]. Potential applications of the work are to modern materials such as homogenised media and composites with tunable parameters, including nanotubes [12,13] and metamaterials [14–16]. One recent application is to the design of a pressure pulsation dampener made of a material with zero or negative Poisson's ratio [17].

The paper is arranged as follows. Section 2 gives the dispersion relation forming the foundation of the work and obtains from it a double series ansatz in Poisson's ratio and the dimensionless thickness. This gives the dominant balance and scaled Poisson's ratio $\tilde{\nu}$. Section 3 determines the arc of negative group velocity, especially its uppermost point in the (frequency, wavenumber) plane, referred to as the critical point. In §4 the range of Poisson's ratio for which backward propagation can occur is determined explicitly, and in §5 the frequency overhang is defined and plotted. Section 6 gives the coordinates of various extrema of wavenumber and frequency which are evident in plots. Conclusions are presented in §7, including some promising directions for further research.

2. The dispersion relation

Here we give the definitions in [1] required for the dispersion relation. The elastic displacement satisfies Navier's equation with wave speeds

$$c_1 = \left\{ \frac{1 - \nu}{(1 + \nu)(1 - 2\nu)} \right\}^{1/2} c_0, \quad c_2 = \frac{c_0}{\{2(1 + \nu)\}^{1/2}}, \quad (2.1)$$

in which ν is Poisson's ratio and $c_0 = (E/\rho)^{1/2}$, where E is Young's modulus and ρ is the density. The mean radius of the wall is a and its thickness is h , so that the inner radius is $a_i = a - h/2$ and the exterior radius is $a_e = a + h/2$. Much of what follows is a parameter study in ν and the dimensionless thickness $\epsilon = h/a$, taken to lie in the ranges $-1 < \nu < 1/2$ and $0 < \epsilon < 2$. In

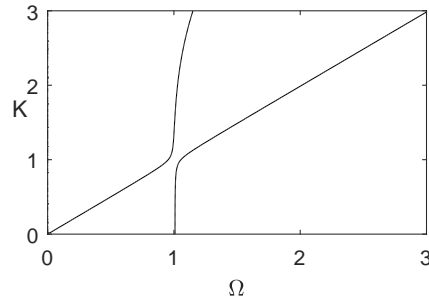


Figure 1. Dispersion relation near the ring frequency for Poisson's ratio $\nu = 0.1$ and dimensionless wall thickness $\epsilon = 0.25$. The near-vertical line extends upwards from the ring frequency to the avoided crossing.

many formulae, the limit $\nu \rightarrow 1/2$ represents an incompressible medium. Other quantities are the wave frequency ω , with dimensionless form $\Omega = \omega a/c_0$; displacement $\mathbf{u} = (u, v, w)$ in cylindrical coordinates (r, θ, z) ; and time t . The tube wall occupies $a_i < r < a_e$, and the axis of the tube is the z -axis. We consider axisymmetric waves with no circumferential displacement, i.e. $v = 0$, and take traction-free boundaries at $r = a_i$ and $r = a_e$. The wave displacements are assumed proportional to $e^{-i\omega t + ikz}$, and this factor is omitted throughout.

The dispersion relation is expressible in terms of Bessel functions J_0 and Y_0 evaluated at $\tilde{\Omega}_1 = \tilde{\Omega}_1(r) = \{(\omega r/c_1)^2 - (kr)^2\}^{1/2}$ and $\tilde{\Omega}_2 = \tilde{\Omega}_2(r) = \{(\omega r/c_2)^2 - (kr)^2\}^{1/2}$. We shall use a subscript 1 or 2 to indicate whether $\tilde{\Omega}_1$ or $\tilde{\Omega}_2$ is required, so that $J_{0,2} = J_0(\tilde{\Omega}_2)$, for example. Either branch of the square roots is permissible, because the dispersion relation has no branch points (i.e. the square roots occur in pairs). The values of r occurring in the boundary conditions are a_i and a_e . Four functions which emerge are

$$d^J(\tilde{\Omega}, K) = \frac{1}{2}(\tilde{\Omega}_2^2 - K^2)J_0(\tilde{\Omega}) + \tilde{\Omega}J_0'(\tilde{\Omega}), \quad (2.2)$$

$$e^J(\tilde{\Omega}, K) = \tilde{\Omega}\{\tilde{\Omega}J_0(\tilde{\Omega}) + J_0'(\tilde{\Omega})\}, \quad (2.3)$$

$$f^J(\tilde{\Omega}, K) = -K^2\tilde{\Omega}J_0'(\tilde{\Omega}), \quad (2.4)$$

$$g^J(\tilde{\Omega}, K) = \frac{1}{2}(\tilde{\Omega}^2 - K^2)\tilde{\Omega}J_0'(\tilde{\Omega}), \quad (2.5)$$

and similarly (d^Y, e^Y, f^Y, g^Y). These are evaluated at the dimensionless frequencies

$$\tilde{\Omega}_{1i} = \tilde{\Omega}_1(a_i), \quad \tilde{\Omega}_{1e} = \tilde{\Omega}_1(a_e), \quad \tilde{\Omega}_{2i} = \tilde{\Omega}_2(a_i), \quad \tilde{\Omega}_{2e} = \tilde{\Omega}_2(a_e) \quad (2.6)$$

and wavenumbers $(K_i, K_e) = (ka_i, ka_e)$ as indicated by subscripts; for example,

$$d_{1i}^J = d^J(\tilde{\Omega}_{1i}, K_i), \quad g_{2e}^Y = g^Y(\tilde{\Omega}_{2e}, K_e). \quad (2.7)$$

In the definition (2.2), the quantity $\tilde{\Omega}_2^2$ is not an argument of the function d^J (nor of d^Y); it is evaluated at $\tilde{\Omega}_{2i}$ or $\tilde{\Omega}_{2e}$, always with a subscript 2.

The result of applying the boundary conditions, and requiring a non-trivial solution, is the determinant equation

$$\begin{vmatrix} d_{1i}^J & d_{1i}^Y & e_{2i}^J & e_{2i}^Y \\ d_{1e}^J & d_{1e}^Y & e_{2e}^J & e_{2e}^Y \\ f_{1i}^J & f_{1i}^Y & g_{2i}^J & g_{2i}^Y \\ f_{1e}^J & f_{1e}^Y & g_{2e}^J & g_{2e}^Y \end{vmatrix} = 0. \quad (2.8)$$

Regarded as a function of ω and k , this is the dispersion relation for the problem we are considering. Details of the steps omitted here may be found in [1].

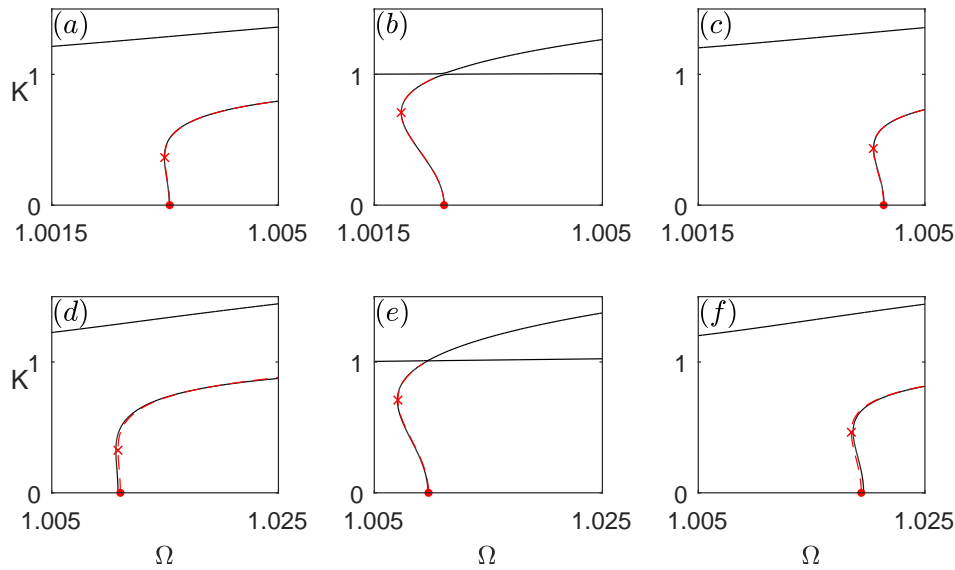


Figure 2. Dispersion curves showing the overhang region between the critical point (\times) and ring frequency point (\cdot) for $\epsilon = 0.25$ (top row) and $\epsilon = 0.5$ (bottom row). The difference between the frequencies at these two points is called ‘the overhang’. In each row, ν increases from left to right, passing from negative to positive values. The exact dispersion relation (2.8) is plotted as a solid black line, and the series form (2.14) as a red dash-dotted line. The cross marks the critical point (K_c, Ω_c) , with K_c taken to order ϵ^2 from (3.6), and Ω_c to order ϵ^4 from (3.8). Values of (ν, ϵ) are (a) $(-0.05, 0.25)$; (b) $(0.001, 0.25)$; (c) $(0.05, 0.25)$; (d) $(-0.1, 0.5)$; (e) $(0.001, 0.5)$; (f) $(0.1, 0.5)$. In (3.6) and (3.8), the corresponding values of $\tilde{\nu}$ have been used. See figure 3(c, f) for the locus of all possible positions of the critical point when ν or $\tilde{\nu}$ varies while ϵ is held constant.

(a) Numerical plots of the dispersion relation

Our concern in this paper is the form of the dispersion relation near the first cut-on frequency, known as the ring frequency. Figure 1 shows the dispersion curve for real (Ω, K) for $\nu = 0.1$, $\epsilon = 0.25$, computed numerically from (2.8) to machine precision. In dimensionless variables, the ring frequency is close to $\Omega = 1$. The straightness and near-vertical slope of the dispersion curve are evident—greater than can be accounted for by the usual square-root dependence with an order-one coefficient. Such a region in the dispersion diagram, where a broad range of wavenumbers occurs in a narrow range of frequencies, produces a resonant response in which the amplitude depends strongly on the narrowness of the frequency range.

Figure 2 presents a blow-up of the dispersion curves for $\nu = (-0.05, 0.001, 0.05)$ when $\epsilon = 0.25$, and for $\nu = (-0.1, 0.001, 0.1)$ when $\epsilon = 0.5$, all computed to machine precision. These and similar plots which cover the whole (ν, ϵ) parameter space demonstrate numerically that for all ϵ there is an interval of values of ν for which the dispersion curve slopes backwards from the ring-frequency point $(\Omega, K) = (\Omega_0, 0)$. This interval contains $\nu = 0$, and its width increases with ϵ . The interval always contains both positive and negative ν . Given these numerical results, the task of this paper is to explain them analytically, with an emphasis on finding scaling laws in ν and ϵ which describe all aspects of the backward-sloping region to high accuracy using only simple formulae.

(b) Analytic structure and the ring series

At first sight, the determinant (2.8) is of forbidding analytic complexity, because of the large number of logarithmic terms arising from the Bessel functions Y_0 and Y_0' . Nevertheless, the Wronskian analysis in [1] shows that its series expansion in ϵ has a simple form in which no Bessel functions or logarithms appear. This form is

$$a_0 + a_2\epsilon^2 + a_4\epsilon^4 + \dots = 0, \quad (2.9)$$

where the coefficients a_0, a_2, \dots are polynomials in the dimensionless frequency $\Omega = \omega a/c_0$ and dimensionless wavenumber $K = ka$. These polynomials are exact; that is, they are not truncations of infinite series, and they may rapidly be determined from (2.8). This is the original contribution of [1]. The coefficients of the polynomials contain ν as a parameter, but in a simple way: each coefficient is either an integer or a ratio of polynomials in ν with integer coefficients.

For our purposes, a two-stage transformation of (2.9) is convenient. First, we use the exact factorisation when $\nu = 0$ to obtain the equivalent form

$$\begin{aligned} (\Omega^2 - K^2) \{ \Omega^2 - 1 + \epsilon^2(p_{20} + \nu p_{21}) + \epsilon^4(p_{40} + \nu p_{41}) + \dots \} \\ = \nu^2 \{ \Omega^4 + \sum_{n=0}^{\infty} \nu^n (\epsilon^2 q_{2,n} + \epsilon^4 q_{4,n} + \dots) \}, \end{aligned} \quad (2.10)$$

in which the factor $\Omega^2 - K^2$ is explicit, and a double series form in ν and ϵ is adopted (we omit commas between subscripts when this is clear). The quantities p_{mn} and q_{mn} are polynomials in Ω^2 and K^2 with rational coefficients. For example, $p_{21} = -\Omega^2(2\Omega^2 - K^2)/6$. Second, we invert (2.10) analytically about the point $\Omega = 1$ to obtain the ring series

$$\Omega^2 = 1 + A_{02}\nu^2 + A_{04}\nu^4 + \dots + \sum_{n=0}^{\infty} \nu^n (\epsilon^2 A_{2,n} + \epsilon^4 A_{4,n} + \dots), \quad (2.11)$$

where the coefficients A_{mn} are functions of K^2 . Only even powers of ν occur in the ϵ^0 terms. A short Mathematica code gives

$$A_{02} = \frac{1}{1 - K^2}, \quad A_{04} = \frac{1 - 2K^2}{(1 - K^2)^3}, \quad A_{20} = \frac{1}{12} \{1 - K^2(1 - K^2)\}, \quad A_{21} = \frac{1}{3} \left(1 - \frac{1}{2}K^2\right), \quad (2.12)$$

$$A_{22} = \frac{5 - 10K^2 + 8K^4 - 5K^6 + K^8}{12(1 - K^2)^2}, \quad A_{40} = -\frac{1}{720} (15 + 12K^2 - 24K^4 + 17K^6), \quad (2.13)$$

and so on [1]. These coefficients are exact. The A_{mn} are rational functions of K^2 in which the degree of the numerator increases steadily with m and n , and the denominator is a power of $1 - K^2$. The coefficients for $n = 0$ or 1 (and no others) are polynomials in K^2 . An alternative form of the ring series is the square root of (2.11), which is

$$\begin{aligned} \Omega = 1 + \frac{1}{2} (A_{20}\epsilon^2 + A_{02}\nu^2) + \frac{1}{2} A_{21}\epsilon^2\nu \\ + \frac{1}{2} \left\{ (A_{40} - \frac{1}{4}A_{20}^2)\epsilon^4 + (A_{22} - \frac{1}{2}A_{20}A_{02})\epsilon^2\nu^2 + (A_{04} - \frac{1}{4}A_{02}^2)\nu^4 \right\} + \dots \end{aligned} \quad (2.14)$$

The displayed terms are plotted as the red dash-dotted curves in figure 2 for a range of values of (ν, ϵ) . It can be seen that the accuracy is excellent, even for $\epsilon = 0.5$.

(c) Poisson scaling

Our aim is to describe analytically how the dispersion curve varies with ν at fixed ϵ . To this end, we adopt the method of dominant balances [6–8] in which a scaling is chosen to maximise the number of terms in balance at leading order. Here, this occurs if we take Ω and K to be of order one, and ν to be formally of the same order as ϵ . Thus we define a scaled Poisson's ratio $\tilde{\nu} = \sqrt{12}\nu/\epsilon$, in which the factor $\sqrt{12}$ is for numerical convenience. Our procedure is to write

formulae in terms of $(\tilde{\nu}, \epsilon)$, rather than (ν, ϵ) , and in series expansions regard $\tilde{\nu}$ as being formally of order one. We call this approach Poisson scaling, since it depends on the dominant balance $\nu \sim \epsilon$. Thus on substituting $\nu = \tilde{\nu}\epsilon/\sqrt{12}$ into (2.11), and re-ordering, we obtain

$$\begin{aligned} \Omega^2 = 1 + \frac{\epsilon^2}{12} \left\{ 1 - K^2(1 - K^2) + \frac{\tilde{\nu}^2}{1 - K^2} \right\} + \frac{\tilde{\nu}\epsilon^3}{3\sqrt{12}} \left(1 - \frac{1}{2}K^2 \right) \\ + \epsilon^4 \left\{ A_{40}(K^2) + \frac{\tilde{\nu}^2}{12} A_{22}(K^2) + \frac{\tilde{\nu}^4}{144} A_{04}(K^2) \right\} + \dots, \end{aligned} \quad (2.15)$$

with A_{40} , A_{22} , and A_{04} defined as in (2.12)–(2.13). The series (2.14) is already written with Poisson scaling in mind. For example, its last terms combine to into

$$\frac{\epsilon^4}{2} \left\{ \left(A_{40} - \frac{1}{4}A_{20}^2 \right) + \frac{\tilde{\nu}^2}{12} \left(A_{22} - \frac{1}{2}A_{20}A_{02} \right) + \frac{\tilde{\nu}^4}{144} \left(A_{04} - \frac{1}{4}A_{02}^2 \right) \right\}, \quad (2.16)$$

and putting $K = 0$ in the whole series gives the ring frequency Ω_0 in the form

$$\Omega_0 = \Omega_0(\tilde{\nu}, \epsilon) = 1 + \frac{\epsilon^2}{24}(1 + \tilde{\nu}^2) + \frac{\tilde{\nu}\epsilon^3}{6\sqrt{12}} + \frac{\epsilon^4}{1152}(-13 + 18\tilde{\nu}^2 + 3\tilde{\nu}^4) + \dots \quad (2.17)$$

3. The critical point

Figure 2 shows that depending on (ν, ϵ) , or equivalently $(\tilde{\nu}, \epsilon)$, the branch of the dispersion curve extending upwards from $(\Omega_0, 0)$ may tilt backwards up to a critical point marked with a cross, where $d\Omega/dK = 0$, beyond which it slopes forward. This point will be denoted (Ω_c, K_c) , where Ω_c is the critical frequency and K_c is the critical wavenumber. To determine their values, we use the fact that K_c^2 is a root of $d(\Omega^2)/d(K^2) = 0$, regarded as an equation in K^2 , and from (2.15) we have

$$\begin{aligned} \frac{d(\Omega^2)}{d(K^2)} = \frac{\epsilon^2}{12} \left\{ -1 + 2K^2 + \frac{\tilde{\nu}^2}{(1 - K^2)^2} \right\} - \frac{\tilde{\nu}\epsilon^3}{6\sqrt{12}} \\ + \epsilon^4 \left\{ A'_{40}(K^2) + \frac{\tilde{\nu}^2}{12} A'_{22}(K^2) + \frac{\tilde{\nu}^4}{144} A'_{04}(K^2) \right\} + \dots \end{aligned} \quad (3.1)$$

Here primes denote derivatives with respect to K^2 . This gives an expansion in powers of ϵ of the form

$$K_c^2 = K_c^2(\tilde{\nu}, \epsilon) = K_{c0}^2(\tilde{\nu}) + \epsilon(K_c^2)_1(\tilde{\nu}) + \epsilon^2(K_c^2)_2(\tilde{\nu}) + \dots, \quad (3.2)$$

where K_{c0}^2 and $(K_c^2)_2$ are even functions of $\tilde{\nu}$, and $(K_c^2)_1$ is odd. A feature of (3.2) (and most series we use) is that it contains odd as well as even powers of ϵ ; this is a consequence of Poisson scaling, in which $\tilde{\nu}$ instead of ν is used as a parameter, and terms are ordered with $\tilde{\nu}$ regarded as order one.

(a) Calculation of the critical wavenumber

On substituting the series form of K_c^2 into (3.1), and equating coefficients of successive powers of ϵ to zero, we obtain

$$(1 - K_{c0}^2)^2 (1 - 2K_{c0}^2) = \tilde{\nu}^2, \quad (3.3)$$

$$(K_c^2)_1 = \frac{\tilde{\nu}}{\sqrt{12}} \left(\frac{1 - K_{c0}^2}{2 - 3K_{c0}^2} \right), \quad (3.4)$$

and a somewhat longer expression for $(K_c^2)_2$. The form of (3.4) makes explicit that $(K_c^2)_1$ is odd in $\tilde{\nu}$. Since (3.3) is a cubic equation in K_{c0}^2 , it may be solved explicitly. The relevant root is $K_{c0}^2 =$

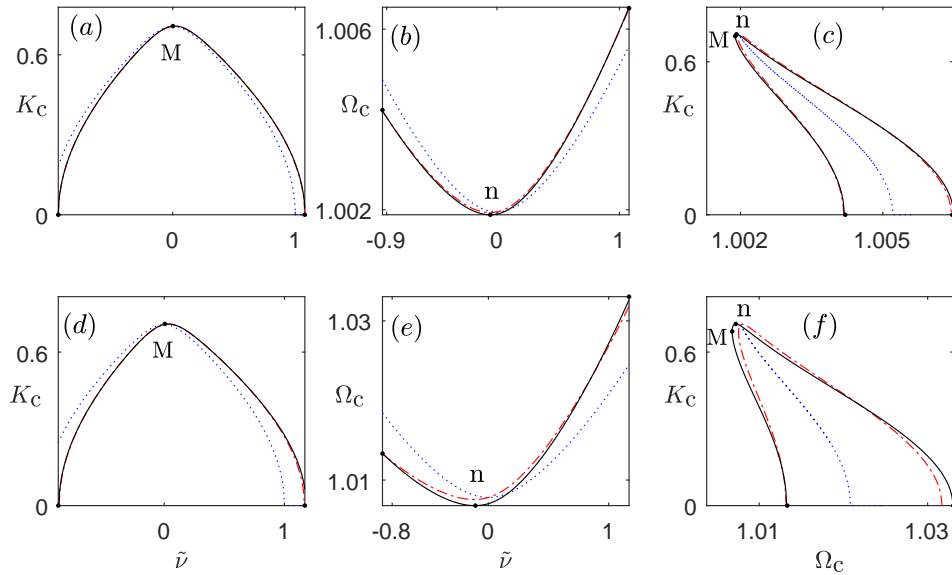


Figure 3. Dependence of critical wavenumber K_c , critical frequency Ω_c , and critical point (Ω_c, K_c) on scaled Poisson's ratio $\tilde{\nu}$ for $\epsilon = 0.25$ (top row) and $\epsilon = 0.5$ (bottom row); the plots show how the coordinates of the crosses in figure 2 vary along a row. The range of $\tilde{\nu}$ on each curve is that for which an overhang exists. Codes for first, second, and third truncations are (blue, dotted), (red, dash-dotted), and (black, solid). (a), (d) Critical wavenumber $K_c(\tilde{\nu}, \epsilon)$ from (3.6). The series to order ϵ^2 (solid curve) are indistinguishable from those to order ϵ , and so hide the dash-dotted curves. (b), (e) Critical frequency $\Omega_c(\tilde{\nu}, \epsilon)$ from (3.8). The end-points $(\tilde{\nu}_{\pm}, \Omega_{c\pm})$ from (4.3) and (4.5) are marked with dots. (c), (f) Locus of critical points $(K_c(\tilde{\nu}, \epsilon), \Omega_c(\tilde{\nu}, \epsilon))$ as $\tilde{\nu}$ varies at fixed ϵ , using the curves in the previous two columns. The lettering in (c, f) corresponds to that in (a, d) and (b, e).

$(5 - \gamma^{1/3} - \gamma^{-1/3})/6$, where

$$\gamma = \gamma(\tilde{\nu}) = 1 + 54\tilde{\nu}^2 + 3\sqrt{12}(\tilde{\nu}^2 + 27\tilde{\nu}^4)^{1/2}. \quad (3.5)$$

The quantities $(K_c^2)_1, (K_c^2)_2, \dots$ may now be found as expressions in $\tilde{\nu}$, using (3.4) and its successor equations. These present no difficulty to Mathematica, and are the basic ingredients for the further series expansions developed in the rest of the paper.

In (3.3), if K_{c0} increases from 0 to $1/\sqrt{2}$, the corresponding value of $\tilde{\nu}^2$ decreases from 1 to 0. Hence in the range $-1 \leq \tilde{\nu} \leq 1$, equation (3.3) defines a symmetric non-negative function $K_{c0}(\tilde{\nu})$ which has a maximum value $K_{c0} = 1/\sqrt{2}$ at $\tilde{\nu} = 0$, and descends to $K_{c0} = 0$ at $\tilde{\nu} = \pm 1$. These values agree with K_{c0} as determined by (3.5). In the original variables (ν, ϵ) , the function $K_{c0}(\tilde{\nu})$ becomes $K_{c0}(\sqrt{12}\nu/\epsilon)$, which is self-similar, so that the series (3.2) has the property of leading-order self-similarity. Thus one advantage of the variable $\tilde{\nu}$ now becomes apparent: it is the self-similarity parameter in situations where the leading-order approximation is good enough. If K_{c0} is regarded as a function of ν rather than $\tilde{\nu}$, the maximum is still $1/\sqrt{2}$, but the relevant range becomes $|\nu| \leq \epsilon/\sqrt{12}$. The fact that $K'_{c0} = 0$ at $\tilde{\nu} = 0$, or equivalently at $\nu = 0$, is used in later series expansions.

For plotting, we use instead of (3.2) the alternative form

$$K_c = K_c(\tilde{\nu}, \epsilon) = K_{c0}(\tilde{\nu}) + \epsilon K_{c1}(\tilde{\nu}) + \epsilon^2 K_{c2}(\tilde{\nu}) + \dots, \quad (3.6)$$

where

$$K_{c1} = \frac{(K_c^2)_1}{2K_{c0}}, \quad K_{c2} = \frac{(K_c^2)_2}{2K_{c0}} - \frac{\{(K_c^2)_1\}^2}{8K_{c0}^3}, \quad \dots \quad (3.7)$$

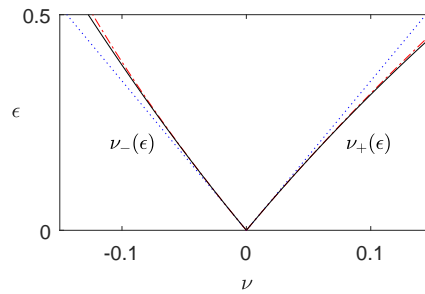


Figure 4. Series expansion (4.4) of the curves $\nu = \nu_{\pm}(\epsilon)$ to orders ϵ (blue dotted), ϵ^2 (red dash-dotted), and ϵ^3 (black solid). An overhang in the dispersion relation exists when (ν, ϵ) lies between these two curves; then backward propagation takes place for (Ω, K) on the arc of the dispersion curve between the critical point (Ω_c, K_c) and the ring-frequency point $(\Omega_0, 0)$, indicated by the symbols \times and \cdot in figure 2.

Here K_{c0} and K_{c2} are even, and K_{c1} is odd. Note that $(K_c^2)_1 \neq K_{c1}^2$ and $(K_c^2)_2 \neq K_{c2}^2$. Figure 3(a, d) shows successive truncations of (3.6) to order 1, ϵ , and ϵ^2 for $\epsilon = 0.25$ (top row) and $\epsilon = 0.5$ (bottom row). Convergence is rapid: the series up to orders ϵ and ϵ^2 are almost indistinguishable on the scale of the plots. The symmetry of the first approximation $K_{c0}(\tilde{\nu})$ (blue dotted curve) is evident, as is the deviation from symmetry in the next two approximations.

(b) The critical frequency

The critical frequency Ω_c is obtained from (2.14), rewritten with $\nu = \tilde{\nu}\epsilon/\sqrt{12}$ as in (2.15)–(2.16), and evaluated at $K = K_c(\tilde{\nu}, \epsilon)$. Its series form is

$$\Omega_c = \Omega_c(\tilde{\nu}, \epsilon) = 1 + \epsilon^2 \Omega_{c2}(\tilde{\nu}) + \epsilon^3 \Omega_{c3}(\tilde{\nu}) + \epsilon^4 \Omega_{c4}(\tilde{\nu}) + \dots, \quad (3.8)$$

in which $\Omega_{c2}(\tilde{\nu}), \Omega_{c3}(\tilde{\nu}), \dots$ are determined by $K_{c0}(\tilde{\nu}), K_{c1}(\tilde{\nu}), \dots$ on the right-hand side of (3.6), which are themselves determined by (3.3)–(3.4) and $(K_c^2)_2$. The function $\Omega_{c0}(\tilde{\nu})$ is symmetric in $\tilde{\nu}$, as it depends only on $K_{c0}(\tilde{\nu})$. Successive truncations of (3.8) are plotted in figure 3(b, e) for $\epsilon = 0.25$ and $\epsilon = 0.5$. Convergence for $\epsilon = 0.25$ is rapid, and only slightly less so for $\epsilon = 0.5$. In the latter case, the exterior radius of the cylinder is three times the inner radius; so the accuracy displayed in the lower row of plots is remarkable for an approximation based on the assumption $\epsilon \ll 1$. This degree of accuracy confirms the power of the dominant balance approach, as implemented here via Poisson scaling.

Figure 3(c, f) combines the plots in the previous two columns to give the curve $(K_c(\tilde{\nu}, \epsilon), \Omega_c(\tilde{\nu}, \epsilon))$ at fixed ϵ , in which $\tilde{\nu}$ is now a parameter, and so is not visible. As $\tilde{\nu}$ increases, the curve is traversed clockwise (except that, by symmetry in $\tilde{\nu}$, the first approximation $(K_{c0}(\tilde{\nu}), \Omega_{c0}(\tilde{\nu}))$ collapses to a line traversed up and down). The interpretation of this curve is that it gives the locus of the points in figure 2 marked with a red cross, i.e. the critical points, when $\tilde{\nu}$ varies at fixed ϵ . It gives all such points.

4. The range of Poisson's ratio for a critical frequency

Figure 3(a, d) indicates that K_c approaches zero as $\tilde{\nu}$ moves away from zero in either direction, so that $K_c = 0$ when $\tilde{\nu}$ takes either of two values which we may denote $\tilde{\nu}_{\pm}(\epsilon)$. Thus we have the defining relation

$$K_c(\epsilon, \tilde{\nu}_{-}(\epsilon)) = K_c(\epsilon, \tilde{\nu}_{+}(\epsilon)) = 0, \quad (4.1)$$

and a critical point (Ω_c, K_c) exists when $\tilde{\nu}$ lies in the range $\tilde{\nu}_{-}(\epsilon) \leq \tilde{\nu} \leq \tilde{\nu}_{+}(\epsilon)$. Since the ring frequency Ω_0 also corresponds to zero wavenumber, it follows that we have the identity $\Omega_c = \Omega_0$ when $\tilde{\nu} = \tilde{\nu}_{\pm}(\epsilon)$; this is a useful check of formulae. When $\tilde{\nu}$ lies outside the range $\tilde{\nu}_{-}(\epsilon)$ to

$\tilde{\nu}_+(\epsilon)$, there is no critical point, because the branch of the dispersion curve emerging from the ring frequency ascends to the right everywhere.

To determine $\tilde{\nu}_\pm(\epsilon)$, we equate the right-hand side of (3.1) to zero at $K = 0$. This gives

$$\tilde{\nu}_\pm^2 - 1 - \frac{\tilde{\nu}_\pm \epsilon}{\sqrt{3}} + \epsilon^2 \left(\frac{\nu_\pm^4}{12} - \frac{1}{5} \right) + O(\epsilon^3) = 0, \quad (4.2)$$

in which there is no term in $\epsilon^2 \tilde{\nu}_\pm^2$ because $A'_{22}(0) = 0$. Hence

$$\tilde{\nu}_\pm = \tilde{\nu}_\pm(\epsilon) = \pm 1 + \frac{\epsilon}{\sqrt{12}} \pm \frac{\epsilon^2}{10} + O(\epsilon^3), \quad (4.3)$$

or equivalently

$$\nu_\pm = \nu_\pm(\epsilon) = \pm \frac{\epsilon}{\sqrt{12}} + \frac{\epsilon^2}{12} \pm \frac{\epsilon^3}{10\sqrt{12}} + O(\epsilon^4). \quad (4.4)$$

The curves $\nu = \nu_\pm(\epsilon)$ are plotted in figure 4. They mark out a wedge-shaped region in the (ν, ϵ) plane for which backward propagation near the ring frequency occurs. Successive truncations of (4.4) can be seen to converge rapidly.

The frequencies corresponding to $\tilde{\nu}_\pm$ may be denoted $\Omega_{c\pm}$. Since they equal the ring frequency evaluated at $\tilde{\nu}_\pm$, they may be calculated by substituting (4.3) into either (2.17) or (3.8). The result by either method is

$$\Omega_{c\pm} = \Omega_{c\pm}(\epsilon) = 1 + \frac{\epsilon^2}{12} \pm \frac{\epsilon^3}{4\sqrt{12}} + \frac{47\epsilon^4}{1440} + O(\epsilon^5). \quad (4.5)$$

These frequencies are marked as dots at the ends of the solid black Ω_c curves in figure 3(b, e) and the (Ω_c, K_c) curves in figure 3(c, f). They differ by an amount $\Omega_{c+} - \Omega_{c-} = \epsilon^3/(2\sqrt{12}) + O(\epsilon^5)$, which is a measure of the asymmetry of the Ω_c curves and the distance apart of the ends of the (Ω_c, K_c) curves.

5. The frequency overhang

The difference between Ω_0 and the critical frequency Ω_c is a measure of the flatness of the dispersion curve in the frequency range (Ω_c, Ω_0) , and so is an important factor in the resonant response in this range. We shall use the term frequency overhang for the positive quantity $\Omega_0 - \Omega_c$, but in plots display its negative $\Omega_{dc} = \Omega_c - \Omega_0 = \Omega_c(\tilde{\nu}, \epsilon) - \Omega_0(\tilde{\nu}, \epsilon)$.

Figure 5(a, c) shows Ω_{dc} as function of $\tilde{\nu}$ for $\epsilon = 0.25$ and $\epsilon = 0.5$. Here a check is the exact value $\Omega_{dc} = 0$ when $\tilde{\nu} = \tilde{\nu}_\pm(\epsilon)$, because then $\Omega_c = \Omega_0$, noted in §4. Similarly, the curves $(\Omega_{dc}(\tilde{\nu}), K_{dc}(\tilde{\nu}))$ shown in (b, d) must begin and end at $(0, 0)$, where $\tilde{\nu} = \tilde{\nu}_\pm(\epsilon)$, so that the curves are loops. In the plots, the smallness of the Ω_{dc} scale, in contrast to the order-one K_c scale, is a measure of the flatness of the dispersion curve, as shown in figure 1 with which we started. The ascending and descending parts of a loop would collapse onto a single line if $\Omega_{dc}(\tilde{\nu})$ and $K_{dc}(\tilde{\nu})$ were symmetric in $\tilde{\nu}$. Thus the narrowness of the loops shows that the asymmetry is small. Analytically, Ω_{dc} is the difference between series (2.17) and (3.8). Hence explicit formulae are available, if required, starting with the basic relations (3.3)–(3.5).

6. Extrema on critical curves

Figures 3 and 5 indicate various maxima and minima with the letters M, m, and n. We now determine their coordinates.

(a) The maximum critical wavenumber

A plot of $K_c(\tilde{\nu}, \epsilon)$ as a function of $\tilde{\nu}$ at fixed ϵ , as in figure 3(a, d), attains a maximum K_{cM} at a value $\tilde{\nu} = \tilde{\nu}_M = \tilde{\nu}_M(\epsilon)$. Thus $K_{cM} = K_{cM}(\epsilon) = \max_{\tilde{\nu}} K_c(\tilde{\nu}, \epsilon) = K_c(\tilde{\nu}_M(\epsilon), \epsilon)$, and $\tilde{\nu}_M$ satisfies the

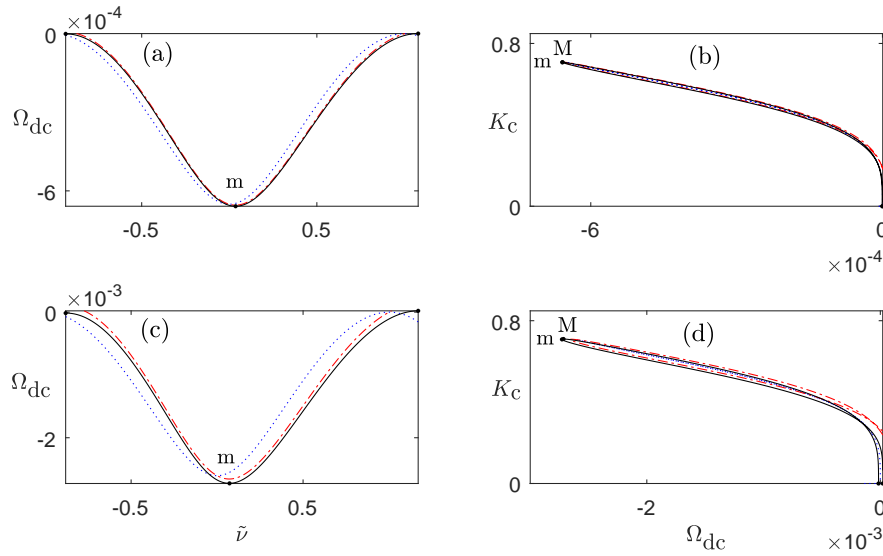


Figure 5. Dependence of negative frequency overhang $\Omega_{dc} = \Omega_d - \Omega_0$ and the point (Ω_{dc}, K_c) on scaled Poisson's ratio $\tilde{\nu}$ for $\epsilon = 0.25$ (top row) and $\epsilon = 0.5$ (bottom row); the series used are (6.8), (2.17), and (3.6), and the codes indicating the first, second, and third truncations are (blue, dotted), (red, dash-dotted), and (black, solid), as in figure 3. The small inaccuracy at the lower right of (d), where the exact curve passes through the origin, is from neglected $O(\epsilon^5)$ terms. These start to become important for $\epsilon \geq 0.5$.

equation

$$K'_{c0}(\tilde{\nu}_M) + \epsilon K'_{c1}(\tilde{\nu}_M) + \epsilon^2 K'_{c2}(\tilde{\nu}_M) + \dots = 0, \quad (6.1)$$

from (3.6). On substituting $\tilde{\nu}_M = \tilde{\nu}_{M0} + \epsilon \tilde{\nu}_{M1} + \epsilon^2 \tilde{\nu}_{M2} + \dots$, and equating the coefficients of successive powers of ϵ to zero, we obtain

$$K'_{c0} = 0, \quad K''_{c0} \tilde{\nu}_{M1} = -K'_{c1}, \quad K''_{c0} \tilde{\nu}_{M2} = -K'_{c2} - K''_{c1} \tilde{\nu}_{M1}^2 - \frac{1}{2} K'''_{c0} \tilde{\nu}_{M1}^2, \quad (6.2)$$

and so on, with derivatives evaluated at $\tilde{\nu}_{M0}$. From the parities of K_{c0} , K_{c1} , and K_{c2} noted after (3.7), it follows that $\tilde{\nu}_{M0} = 0$ and $\tilde{\nu}_{M2} = 0$. Then (3.3)–(3.4) give $\tilde{\nu}_{M1} = 1/(4\sqrt{12})$, so that $\tilde{\nu}_M = \epsilon/(4\sqrt{12}) + O(\epsilon^3)$, or equivalently $\nu_M = \epsilon^2/48 + O(\epsilon^4)$. Hence substituting $\tilde{\nu}_M$ into series (3.6) for K_c , and using $\tilde{\nu}_{M0} = 0$, we obtain

$$K_{cM} = K_{c0}(0) + \epsilon^2 \left\{ \frac{1}{2} K''_{c0}(0) \tilde{\nu}_{M1}^2 + K'_{c1}(0) \tilde{\nu}_{M1} + K_{c2}(0) \right\} + O(\epsilon^4). \quad (6.3)$$

The coefficients here may be read off from the Taylor expansions

$$K_{c0}(\tilde{\nu}) = \frac{1}{\sqrt{2}} - \sqrt{2} \tilde{\nu}^2 + 7\sqrt{2} \tilde{\nu}^4 + O(\tilde{\nu}^6), \quad (6.4)$$

$$K_{c1}(\tilde{\nu}) = \frac{\tilde{\nu}}{2\sqrt{6}} - \frac{\sqrt{3}}{\sqrt{2}} \tilde{\nu}^3 + O(\tilde{\nu}^5), \quad (6.5)$$

$$K_{c2}(\tilde{\nu}) = \frac{1}{160\sqrt{2}} - \frac{17}{80\sqrt{2}} \tilde{\nu}^2 + O(\tilde{\nu}^4), \quad (6.6)$$

obtainable from (3.7). These give $K_{c0}(0) = 1/\sqrt{2}$, $K''_{c0}(0) = -2\sqrt{2}$, $K'_{c1}(0) = 1/(2\sqrt{6})$, and $K_{c2}(0) = 1/(160\sqrt{2})$, from which

$$K_{cM} = \frac{1}{\sqrt{2}} + \frac{1}{60\sqrt{2}} \epsilon^2 + O(\epsilon^4), \quad \Omega_{cM} = 1 + \frac{\epsilon^2}{32} - \frac{287}{30720} \epsilon^4 + O(\epsilon^5). \quad (6.7)$$

(b) The minimum critical frequency

The critical frequency $\Omega_c(\tilde{\nu}, \epsilon)$, regarded as a function of $\tilde{\nu}$ at fixed ϵ , has a minimum $\Omega_{cn} = \Omega_{cn}(\epsilon)$ at $\tilde{\nu} = \tilde{\nu}_n = \tilde{\nu}_n(\epsilon)$. This occurs for $|\tilde{\nu}| \ll 1$, so that (6.4)–(6.6) may be used at the outset in the expansion (3.6) of K_c . Then (2.14), written with $\nu = \tilde{\nu}\epsilon/\sqrt{12}$ and evaluated at $K = K_c$, becomes

$$\Omega_c(\tilde{\nu}) = 1 + \epsilon^2 \left(\frac{1}{32} + \frac{\tilde{\nu}^2}{12} - \frac{\tilde{\nu}^4}{6} + \dots \right) + \epsilon^3 \left(\frac{\tilde{\nu}}{16\sqrt{3}} + \frac{\tilde{\nu}^3}{12\sqrt{3}} - \frac{2\tilde{\nu}^5}{3\sqrt{3}} + \dots \right) + O(\epsilon^4), \quad (6.8)$$

from which

$$\Omega'_c(\tilde{\nu}) = \epsilon^2 \left(\frac{\tilde{\nu}}{6} - \frac{2\tilde{\nu}^3}{3} + \dots \right) + \epsilon^3 \left(\frac{1}{16\sqrt{3}} - \frac{\tilde{\nu}^2}{4\sqrt{3}} + \dots \right) + O(\tilde{\nu}\epsilon^4). \quad (6.9)$$

Solving $\Omega'_c(\tilde{\nu}_n) = 0$ as a series in ϵ , we find $\tilde{\nu}_n = -\sqrt{3}\epsilon/8 + O(\epsilon^3)$, or equivalently $\nu_n = -\epsilon^2/16 + O(\epsilon^4)$. Then substituting into (6.8) including the $O(\epsilon^4)$ term, and (3.6) we obtain

$$\Omega_{cn} = 1 + \frac{\epsilon^2}{32} - \frac{1501}{92160}\epsilon^4 + \dots, \quad K_{cn} = \frac{1}{\sqrt{2}} - \frac{3}{20\sqrt{2}}\epsilon^2 + O(\epsilon^3). \quad (6.10)$$

The points M and n are marked on the (Ω_c, K_c) curve in figure 3(c, f). For small ϵ , the points are hard to distinguish, because of the small radius of curvature near the top of the curve.

(c) The maximum overhang

Recall that $\Omega_{dc} = \Omega_c - \Omega_0$ is a negative quantity by definition. For fixed ϵ , the maximum overhang corresponds to the minimum $\Omega_{dcm} = \Omega_{dcm}(\epsilon)$ of Ω_{dc} , attained at a value $\tilde{\nu} = \tilde{\nu}_m = \tilde{\nu}_m(\epsilon)$ of order $O(\epsilon)$. To determine $\tilde{\nu}_m$, we first subtract the series (2.17) for Ω_0 from (6.8) for Ω_c to obtain

$$\Omega_{dc}(\tilde{\nu}) = \epsilon^2 \left(-\frac{1}{96} + \frac{\tilde{\nu}^2}{24} - \frac{\tilde{\nu}^4}{6} + \dots \right) + \epsilon^3 \left(-\frac{\tilde{\nu}}{48\sqrt{3}} + \frac{\tilde{\nu}^3}{12\sqrt{3}} - \frac{2\tilde{\nu}^5}{3\sqrt{3}} + \dots \right) + O(\epsilon^4), \quad (6.11)$$

whence

$$\Omega'_{dc}(\tilde{\nu}) = \epsilon^2 \left(\frac{\tilde{\nu}}{12} - \frac{2\tilde{\nu}^3}{3} + \dots \right) + \epsilon^3 \left(-\frac{1}{48\sqrt{3}} + \frac{\tilde{\nu}^2}{4\sqrt{3}} + \dots \right) + O(\tilde{\nu}\epsilon^4). \quad (6.12)$$

The solution of $\Omega'_{dc}(\tilde{\nu}_m) = 0$ is $\tilde{\nu}_m = \epsilon/(4\sqrt{3}) + O(\epsilon^3)$, or equivalently $\nu_m = \epsilon^2/24 + O(\epsilon^4)$. Substitution into (6.11) and (3.6) gives

$$\Omega_{dcm} = -\frac{\epsilon^2}{96} - \frac{181}{92160}\epsilon^4 + \dots, \quad K_{cm} = \frac{1}{\sqrt{2}} + \frac{\epsilon^2}{160\sqrt{2}} + \dots \quad (6.13)$$

The points M and m are marked on the (Ω_{dc}, K_{dc}) curve in figures 5(b, d), although they are extremely close. The curve starts at (0, 0) for $\tilde{\nu} = \tilde{\nu}_-$, passes through (Ω_{dcM}, K_{cM}) and (Ω_{dcm}, K_{cm}) in that order, and returns to (0, 0) at $\tilde{\nu} = \tilde{\nu}_+$. The curve is traversed anti-clockwise as $\tilde{\nu}$ increases, in contrast to the (Ω_c, K_c) curve in figure 3(c, f), which is traversed clockwise. As pointed out in §5, the separation between the rising and falling parts of the curve is a measure of asymmetry in Poisson's ratio, here rather small. On the curve for $\epsilon = 0.5$, a small inaccuracy is visible near the origin, due to neglected $O(\epsilon^5)$ terms; the exact curve joins up to form a loop.

7. Conclusion

This paper shows that the method of Wronskian identities developed in [1] is powerful enough to describe backward wave propagation in practically unlimited analytical detail, without any loss of mathematical rigour. The crucial point is that the series expansions we have presented, including all displayed coefficients, are exact, in that they are consequences of the dispersion relation (2.8), derived from the linear elastic equations without any kinematic assumptions about the shape of the wave field. These series are new.

Backward propagation near the ring frequency is not captured by traditional thin-shell theories, for example the Novozhilov-Goldenvizer and Donnell-Mushtari approximation [9,19]. The question therefore arises of whether such propagation is captured by thick shell theories, and if so, whether it is captured accurately. Such theories include the effect of transverse shear and rotary inertia. This matter does not appear to have been investigated. We have simplified and re-plotted the results given in a classical work in this area (Naghdi & Cooper [20]), and found that they do indeed capture backward propagation, together with the merging and reconnection of complex wavenumber branches at critical points. The details will be reported elsewhere. Provisionally, we have found that the Naghdi–Cooper equations, with suitable modifications, are more accurate and are valid to higher frequencies than might be supposed. We therefore see a greater role emerging for these equations, and their variants, than hitherto. Moreover, we have found that such equations have previously unidentified factorisation properties, which suggests that the range may be extended still further by the use of finite-product approximations [2,21]. Thus there is currently a lot of life in this classical subject.

An important feature of our method is the explicit dependence on parameters which it yields in all formulae. Thus it is potentially applicable to parametric studies of tunable metamaterials and nanotubes, for example [12,13], and also to a possible type of pressure pulsation damper which operates at vanishingly small or negative Poisson's ratio [17]. Our results suggest that if a driving frequency is increased through the critical frequency, the onset of wave propagation will be rapid when Poisson's ratio is small, and a wide range of wavenumbers will be excited almost simultaneously; alternatively, under broadband forcing one may expect a sharper resonance than normal near the critical frequency. The consequences of such operating characteristics are yet to be determined.

Another current research area is the dynamics of soft elastic tubes as a key component of the biomechanics of nerves and blood vessels [10,11], especially in the medical context. Perhaps surprisingly in such a numerically oriented subject, an analytical solution of the incremental boundary-value problem has been found which involves Bessel functions [11]. There is scope here to extend our approach to include parametric dependence on pre-stress, which dramatically affects the ring frequency. One matter for investigation here would be the range of pre-stress for which a regime of negative group velocity still exists, and how this relates to the localised bifurcation theory developed in [10].

Authors' Contributions. Both of the authors have contributed substantially to the paper.

Competing Interests. We declare that we have no competing interests.

Funding. The work was funded by Keele and Aalborg Universities.

Acknowledgements. The authors thank J. D. Kaplunov, Y. Fu, and D. Emery for helpful comments.

References

1. Chapman CJ, Sorokin SV. 2021 A Wronskian method for elastic waves propagating along a tube. *Proc. R. Soc. Lond. A* **477**, 20210202. (doi:10.1098/rspa.2021.0202)
2. Sorokin SV, Gautier F, Pelat A. 2020 A hierarchy of models of axisymmetric wave propagation in a fluid-filled periodic cylindrical shell composed of high-contrast cells. *Mech. Syst. Signal Proc.* **136**, 106487. (doi.org/10.1016/j.ymsp.2019.106487)
3. Mindlin RD. 1955 An introduction to the mathematical theory of vibrations of elastic plates. Signal Corps Engineering Laboratories, Project 142B. Fort Monmouth: NJ.
4. Shuvalov AL, Poncelet O. 2008 On the backward Lamb waves near thickness resonances in anisotropic plates. *Int. J. Solids and Structures* **45**, 3430–3448. (doi:10.1016/j.ijsolstr.2008.02.004)
5. Sorokin SV. 2003 An introduction to the theory of wave propagation in elastic cylindrical shells filled with an acoustic medium. Institute of Machine Acoustics, Project B1, pp. 1–42. Aalborg University, Denmark.
6. Bender CM, Orszag SA. 1978 *Advanced mathematical methods for scientists and engineers*. New York: McGraw-Hill.

7. Hinch EJ. 1991 *Perturbation methods* Cambridge: CUP. (doi.org/10.1017/CBO9781139172189)
8. Chapman CJ, Wynn HP. 2021 Fractional power series and the method of dominant balances. *Proc. R. Soc. Lond. A* **477**, 20200646. (doi:10.1098/rspa.2020.0646)
9. Novozhilov VV. 1964 *Thin shell theory*. 2nd edn. Groningen: Noordhoff.
10. Emery D, Fu Y. 2021 Localised bifurcation in soft cylindrical tubes under axial stretching and surface tension. *Int. J. Solids and Structures* **219–220**, 23–33. (doi:10.1016/j.ijsolstr.2021.02.007)
11. Emery D, Fu Y. 2021 Elasto-capillary circumferential buckling of soft tubes under axial loading: existence and competition with localised beading and periodic axial modes. *Mechanics of Soft Materials* **3:3**, 1–14. (doi:10.1007/s42558-021-00034-x)
12. Andrianov IV, Kaplunov J, Kudaibergenov AK, Manevitch LI. 2018 The effect of a weak nonlinearity on the lowest cut-off frequencies of a cylindrical shell. *Z. Angew. Math. Phys.* **69:7**, 1–12. (doi:10.1007/s00033-017-0902-9)
13. Ege N, Erbaş B, Kaplunov J. 2021 Asymptotic derivation of refined dynamic equations for a thin elastic annulus. *Mathematics and Mechanics of Solids* **26**, 118–132. (doi:10.1177/1081286520944980)
14. Liao G, Luan C, Wang Z, et al. 2021 Acoustic metamaterials: a review of theories, structures, fabrication approaches, and applications. *Adv. Mater. Technol.* **6**, 2000787, 1–29. (doi:10.1002/admt.202000787)
15. Claeys C, Deckers E, Pluymers B, Desmet W. 2016 A lightweight vibro-acoustic metamaterial demonstrator: numerical and experimental investigation. *Mech. Syst. Signal Proc.* **70–71**, 853–880. (doi.org/10.1016/j.ymsp.2015.08.029)
16. Cummer SA, Christensen J, Andrea A. 2016 Controlling sound with acoustic metamaterials. *Nature Reviews Materials* **1**, 16001. (doi:10.1038/natrevmats.2016.1)
17. Sorokin SV. 2021 Pressure pulsation dampeners made of material with zero Poisson's ratio. Aalborg University Report, prepared for the Danish Science Foundation and Nifisk A/S.
18. Morse PM, Feshbach H. 1953 *Methods of theoretical physics, Part II*. New York: McGraw-Hill.
19. Zadeh MN, Sorokin SV. 2013 Comparison of waveguide properties of curved versus straight planar elastic layers. *Mechanics Res. Comm.* **47**, 61–68. (doi:10.1016/j.mechrescomm.2012.09.003)
20. Naghdi PM, Cooper RM. 1956 Propagation of elastic waves in cylindrical shells, including the effects of transverse shear and rotatory inertia. *J. Acoust. Soc. Am.* **28**, 56–63.
21. Chapman CJ, Sorokin SV. 2010 The finite-product method in the theory of waves and stability. *Proc. R. Soc. Lond. A* **466**, 471–491. (doi:10.1098/rspa.2009.0255)